Journal of Artificial Intelligence Practice (2025)
Clausius Scientific Press, Canada

DOI: 10.23977/jaip.2025.080213
ISSN 2371-8412 Vol. 8 Num. 2

An O-OFDM-IM system based on the 3-D constellation map

Feng Zhi, Yinghua Li

Xi'an Mingde Institute of Technology, Xi'an, Shaanxi Province, 710124, China

Keywords: Optical orthogonal frequency division index modulation; 3 D constellation; error rate

Abstract: O-OFDM-IM (Optical Orthogonal Frequency Division Multiplexing with Index Modulation, O-OFDM-IM) adopts the traditional constellation diagram, which will lead to the system error performance cannot achieve the best. Therefore, this paper proposes an O-OFDM-IM scheme based on three-dimensional constellation diagram. Its essence is to reduce the constellation sign error detection rate by increasing the minimum Euclidean distance between the constellation symbols. At the same time, the subcarrier optimization algorithm is introduced to reduce the error probability of the index bit. The results show that the system error performance and transmission rate are significantly improved at large SNR compared with conventional O-OFDM-IM.

1. Introduction

With index modulation (Index Modulation, IM) [1] through some medium index additional information, this part of the information transmission does not need to consume or only very little energy this advantage, scholars combine IM and OFDM [2], put forward OFDM-IM technology, through the subcarrier index additional information significantly increase the system transmission rate, and a large number of silent subcarrier can improve the reliability of the system. Because of the above advantages of OFDM-IM, it has set off a research boom in the field of visible light communication, and achieved remarkable results in [3-5].

In recent years, scholars have turned their research attention to the O-OFDM-IM in wireless optical communication[6]. However, the optical signal is susceptible to the interference of atmospheric turbulence[7], and the additional information of the activator carrier increases the complexity of the receiver detection, and these factors seriously affect the reliability of the system. Therefore, in order to improve reliability, on the one hand, scholars look for the decoding detection algorithm[8] with excellent error performance at the receiving end. Among them, Reference [8] uses the neural network to complete the detection of index information, and reduces the bit error rate under the traditional method of detection algorithm. On the other hand, the mapping scheme [5,9,10] is optimized at the sender. Among them, references [9] and [10] improve code error performance by interleaving and assigning subcarriers respectively. In addition, scholars also proposed generalized asymmetric limit-amplitude light OFDM-IM[11], O-OFDM-DIM[12] based on discrete wavelet transform to improve the transmission rate and improve the performance of error codes. However, the above optimization schemes all start from the perspective of reducing the error probability of subcarrier index, and with

the increase of signal to noise ratio, the system error probability is mostly affected by the constellation sign error detection rate, which leads to the limited improvement of error performance of the above schemes. All the mentioned documents use two-dimensional constellation diagram, which cannot maximize the minimum Euclidean distance, that is, it cannot minimize the probability of symbol misjudgment, resulting in the system unable to reach the optimal reliability.

In view of this, in order to greatly improve the system error performance, this paper extends the constellation symbol from the 2-D plane to the 3-D plane and increases the Euclidean distance between symbols. Based on this, an O-OFDM-IM scheme based on 3-D constellation is proposed to greatly improve the system error performance. Meanwhile, the carrier optimization algorithm is introduced to further reduce the code error rate.

2. The O-OFDM-IM system based on three-dimensional constellation maps

As shown in Figure 1 is the block diagram of the system. Firstly, the optimal subcarrier index mapping combination is obtained through the subcarrier optimization algorithm, and then the binary bit stream by string and conversion is respectively index mapping and 3 D modulation mapping according to the corresponding mapping rules. Where the role of the 3 D modulation map is to increase the Euclidean distance between the symbols. Then, the symbol of the 3 D modulation map is loaded on the active subcarrier, and then the signal is converted into a positive real number signal after merging the data block, which is sent by the laser through the optical antenna. The optical signal transmitted through the atmospheric channel is received by the detector, and the original data is recovered by the Log Likelihood Ratio (LLR) detection algorithm after the transmitter. The subcarrier optimization algorithm and the 3 D constellation diagram are described in detail below.

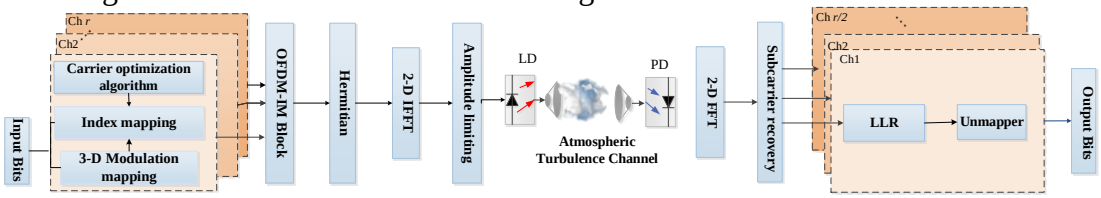

Figure 1 Block diagram of the 3D-O-OFDM-IM system

2.1 Sub-carrier optimization algorithm and three-dimensional constellation diagram

2.1.1 Sub-carrier optimization algorithm

In a traditional O-OFDM-IM system, the g number of subcarriers in the n first subcarrier block is assumed K, and the number of active subcarriers C_n^K is. The number of activator carrier 2^{P_1} combinations $2^{P_1} \le C_n^K$ is, and the actual number of activator carrier combinations is. Usually, there is redundancy in carrier combinations. Because the index mapping adopts the random mapping method, the bit error rate possibly generated by the index mapping is not necessarily minimal. Therefore, this paper makes full use of the redundancy to first select the optimal subcarrier index combination before performing the index mapping, aiming to achieve the minimum subcarrier misdetection rate. Table 1 shows the step diagram of the carrier optimization algorithm.

Table 1 Carrier optimization algorithm

The carrier optimization algorithm
1. Input: number of subcarriers, number of subblocks, number of activator carriers;
2. Output: optimal carrier combination;
3.% Steps
1) Calculate the number of activator carrier combinations; 2) Calculate the sum of the Hamming distance between the combinations;
3) Looking for the maximum combination Z set of Hamming distance; 4) In Z, the number of activator carriers within the most included subcarrier combination is selected as the optimal combination set;
5) finish; 6) Output the optimal carrier combination.

Here is an $n=4,\ K=2,\ P_1=2$ example to illustrate the carrier optimization algorithm. Let the activator carrier be represented by "1" and the silent subcarrier be represented by "0", so 2^{P_1} the possible subcarrier combination $\{0011,0101,1001,0110,1010,1100\}$ is $\mathrm{A}_i=[a_{i1}a_{i2}a_{i3}a_{i4}]$ i=1,2...15 . Then, the set of subcarrier combinations $C_6^4=15$ is, where. The $\mathrm{A}_i=\{1010,0101,1001,0110\}$ selected a_{i1} subcarrier combination set has a common species. If the subcarrier combination set is. Assuming that the selected P subcarrier a_{i1} combination, influenced $\{P^4,P^2,P^2\}$ by the channel $\{4,2,2\}$ characteristics, the receiver may misdetect it into other subcarrier combinations. Let the probability of the subcarrier being misdetected be, then the probability of being detected be other and Hamming distance. It can be seen that the error detection probability is inversely proportional to the Hamming distance between the subcarrier combinations, that is, the larger the Hamming distance, the smaller the error detection probability. Therefore, the Hamming distance between the pairwise combinations in the subcarrier combination set can be calculated separately and summed. Later, the Hamming distance and the largest set from the 15 combined sets were selected as the optimal subcarrier combination. The specific process of the algorithm is:

① Calculate the sum of Hamming distances for pairwise $Q_i=\sum_{e=1}^{4}\sum_{f=1}^{4}d\left(a_{ie},a_{if}\right)$ Q_i $e=1,\cdots,4$ combinations $f=1,\cdots,4$ within $d\left(a_{ie},a_{ij}\right)$15 i sets, i. e.,,. The f e Hamming distance between the first and first subcarrier combinations on the first seed carrier combination set is indicated.

② Take the Hamming distance and the largest B=$\mathrm{A}_{\mathrm{Q}_{\max}}$ combined set as the set of choices. If the sum of the maximum Hamming distance is equal, in order to reduce the probability of error, the far combination between the activator carriers is selected, because the farther the distance between the activator carriers, the less the interference between the subcarriers.

The final optimal combination $\{0101,1001,0110,1010\}$ set is.

2.1.2 3-D constellation map design

In order to increase the minimum European distance between symbols, this paper extends the two-dimensional constellation map in the plane to the three-dimensional surface. According to the distribution characteristics of QAM constellation symbol energy, the appropriate coordinates are selected to maximize the minimum Eodian distance.

Taking 8 QAM as an example, according to the energy distribution characteristics of the 8 QAM constellation, it is divided into two groups according to the amplitude radius of the symbols of the

two rings, build two concentric balls on the three-dimensional surface and construct the cubes on the sphere, then select the vertices of four non-adjacent cubes on each sphere to form the regular tetrahedral constellation. That is, according to the characteristics of 8 QAM sign energy, for the constellation diagram of 3D 8 $\pi/2$QAM, the four nonadjacent vertices of the cube on the inner group are selected to form a regular tetrahedron, the cube on the outer group is selected with four nonadjacent vertices to construct the regular tetrahedron in the same position, and then the regular tetrahedron formed on the outer group is rotated around the z-axis; the 8 vertices are used as the coordinates of 3 D 8 QAM to obtain the coordinates of 3 D-8 QAM.

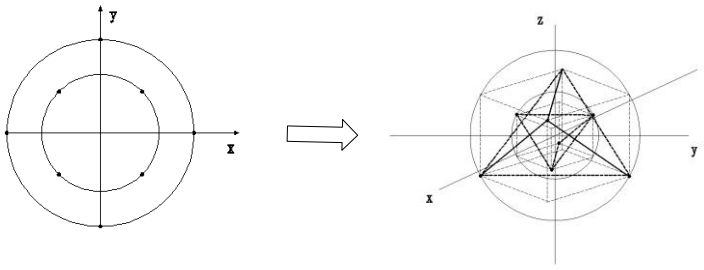

(a) (b)

Figure 2 8 QAM constellation Fig

According to the principle that the larger the Euclidean distance between constellation signs, the smaller the probability of constellation sign error, Figure 2 compares the minimum Euclidean distance (Minimum Euclidean distance, MED) and the mean Euclidean distance of the 2-D and 3-D constellation maps.

Table 2 2-D MED of constellations versus 3-D

constellation	euclidean distance	8QAM
two dimension	minimum	0.81
	average	
three-dimensional	minimum	1.18
	average	1.46

2.2 System model

A system with N subcarriers per frame shall transmit m-bit information once. Where p_1, p_2 m bits is divided into bits and bits, mapped to the activator carrier index number and the constellation symbols sent on the activator carrier, respectively. These N subcarriers K are equally divided into r blocks, with each subcarrier block containing $P_1=\log_2\lfloor C_n^K \rfloor$ n= C_n^K N / r subcarriers. Assuming K that each subcarrier $\lfloor\bullet\rfloor$ block activates the subcarrier, the number of bits transmitted $P_2 = K\cdot 2\log_2(M)$ by the activator carrier $z=\log_2 C_n^K + 2K\log_2(M)$ index on each subcarrier block is, where the combined number of subcarriers selected from n subcarriers represents the downward integration. Let the modulation order be M, then the bits sent by the constellation sign are bits and the total number of binary bits sent by each subcarrier block be bits.

The first subcarrier g block is used as an example to detail g the modulation n process. In the K first subblock, selecting the $I_g=[0,\cdots,\underset{1}{\uparrow}1,\cdots,\underset{K}{\uparrow}1,\cdots 0]$ vector form of the active subcarrier selected

P_2 from the subcarrier $2K$ can be expressed as, where $S_g = s_{g,1},\cdots,s_{g,\alpha},\cdots,s_{g,2K}$ the position of the non-zero element is the activator carrier index number. $\alpha \in (1,2,\cdots 2K), s_{g,\alpha} \in \Re, \Re\widetilde{s_K} = [x_K, y_K, z_K]^T$ Bits are mapped as modulation symbols $\vec{x},\vec{y},\vec{z}$ whose mapping relationships can S_B be represented as. Where is the constellation sign, which can be expressed as a three-dimensional vector, the coordinate values represented by the three elements in the vector. Transfer symbols can be represented as a matrix

$$S_B = \begin{bmatrix} x_0 + jx_1 & x_2 + jx_3 & \ldots & x_{2K-2} + jx_{2K-1} \\ y_0 + jy_1 & y_2 + jy_3 & \ldots & y_{2K-2} + jy_{2K-1} \\ z_0 + jz_1 & z_2 + jz_3 & \ldots & z_{2K-2} + jz_{2K-1} \end{bmatrix} \tag{1}$$

Among, $j = \sqrt{-1}$ The modulation symbol is loaded onto the active subcarrier, and each subcarrier $\varphi' = [\varphi_0 \quad \varphi_1 \quad \ldots \quad \varphi_{N-1}]^T$ block is merged to $\varphi' \in \mathbb{C}^{3\times N}$ generate φ' the OFDM-IM data φ''_{n_1,n_2} block, where. After the hermitian symmetry transformation generation, i. e

$$\varphi^*_{n_1,n_2} = \begin{bmatrix} 0 & \varphi_{x_0} & 0 & \varphi_{x_1} & \ldots & 0 & \varphi_{x_{\frac{N}{4}-1}} & 0 & \varphi^*_{x_{\frac{N}{4}-1}} & \ldots & 0 & \varphi^*_{x_1} & 0 & \varphi^*_{x_0} \\ 0 & \varphi_{y_0} & 0 & \varphi_{y_1} & \ldots & 0 & \varphi_{y_{\frac{N}{4}-1}} & 0 & \varphi^*_{y_{\frac{N}{4}-1}} & \ldots & 0 & \varphi^*_{y_1} & 0 & \varphi^*_{y_0} \\ 0 & \varphi_{z_0} & 0 & \varphi_{z_1} & \ldots & 0 & \varphi_{z_{\frac{N}{4}-1}} & 0 & \varphi^*_{z_{\frac{N}{4}-1}} & \ldots & 0 & \varphi^*_{z_1} & 0 & \varphi^*_{z_0} \end{bmatrix} \tag{2}$$

Where, represents $(\cdot)^*$ the conjugate φ' operation. The inverse two-dimensional Fourier transform can be expressed as

$$\varphi''_{n_1,n_2} = \frac{1}{3N}\sum_{k_1=0}^{2}\sum_{k_2=0}^{N-1}\varphi'_{k_1,k_2}e^{\left[j2\pi(\frac{n_1k_1}{3}+\frac{n_2k_2}{N})\right]} = \frac{1}{3N}\sum_{k_1=0}^{2}e^{\left[j2\pi(\frac{n_1k_1}{3})\right]}\left[\sum_{k_2=0}^{N-1}\varphi'_{k_1,k_2}e^{\left[j2\pi(\frac{n_2k_2}{N})\right]}\right] \tag{3}$$

Where $0 \le n_1 \le 2, 0 \le n_2 \le N-1$ and k_1 represent k_2 the φ' row and column index of the matrix φ''_{n_1,n_2}, respectively. After generating ϕ the time domain symbol, the amplitude limit operation y to form a positive real number signal is sent by the laser through the optical transmitting antenna. Set the receiving signal to

$$y = \eta h \cdot \phi + w \tag{4}$$

$\eta \in [0 \sim 1]$ is the photoelectric conversion efficiency.Under the influence of hermitian symmetry and amplitude limit, the front block signal is directly extracted and doubled. Then the original information can be recovered by detecting it.

At the receiving end, the maximum likelihood detection (Maximum Likelihood, ML) is commonly used, which has excellent code error performance. But when the index bits grow exponentially, using ML brings high complexity. In view of this, $\lambda(\alpha)$ this system selects the LLR algorithm with less complexity. The detection criterion uses the ratio of the subcarrier prior probability to the posterior probability to detect the activator carrier, which can be expressed as

$$\lambda(\alpha)=\ln(K)-\ln(n-K)+\frac{Y'_g(\alpha)}{N_{0,F}}+\ln(\sum_{j=1}^{M}\exp\left|\frac{1}{N_{0,F}}\left\|Y'_g(\alpha)-H^g(\alpha).*S^M(j)\right\|_2^2\right|) \tag{5}$$

Where the $N_{0,F}$ noise power, n the total number of K carriers in the subblock, and $Y'_g(\alpha)$ the g

number α of activated carriers in $H^g(\alpha)$ the g subblock α, representing the receiving S^M signal of the g first carrier in the $\lambda(\alpha)$ subblock α, the channel information of the first carrier in the subblock, and λ the modulation λ symbol. K For the first subblock, the greater the probability that the first carrier is activated. Therefore, by comparing different carriers in the same subblock, the former subcarrier with large absolute value is judged as the activated subcarrier, and then the corresponding constellation sign is recovered according to the estimated activator carrier.

3. Simulation analysis

To verify the feasibility of the proposed scheme, this section performs its simulation verification using the Monte Carlo method, and the results are shown in Figure3-6. The simulation parameters are N=256, the photoelectric conversion coefficient η = 0.5, the modulation order is 8 and 16, and the exponential Weibull channel[13] parameters are shown in Table 3. In the curve description, W and S indicate weak and strong turbulence, respectively, and (n, K) indicate the selection of K activator carriers from the n subcarriers.

Table 3. Parameters of the exponential Weibull turbulence channel

turbulent intensity	Li Tuofu variance	Shape parameter 1	Shape parameter 2	scale parameter	Receive aperture D / mm
weak	0.317	3.67	1.97	0.73	25
stubborn	15.851	5.50	0.74	0.29	25

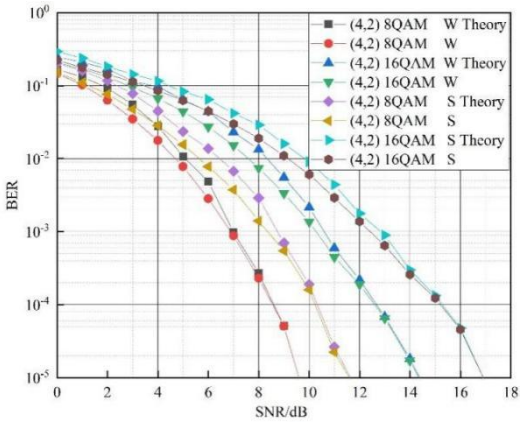

Figure 3 Theoretical and simulation bit error rate of 3D-O-OFDM-IM system

Figure 3 shows the theoretical BER and actual simulation results for the 3D-O-OFDM-IM system. From Figure 3, we show that at the low SNR, the theoretical BER is larger than the experimental simulation results, and the theoretical BER tends to coincide with the experimental simulation results at the high SNR. This is due to the joint bound technique, which derived its upper bit error rate bound. The correctness of the theoretical derivation is illustrated.

Figure 4 shows the influence of modulation order, activator carriers and turbulence on the performance of system error codes. It can be seen from Figure 4: ①When the active carrier number is certain, the increase of the system transmission rate is increased 1×10^{-5} with the increase of the modulation order. However, at this time, the bit error rate of the system will increase accordingly, which is due to the use of high-order modulation and the probability of signal misjudgment. When the bit error rate is, the system SNR loses about 4.5 dB.②When the modulation order is certain, the

transmission rate also increases with the increase of the active carrier number. However, due to the increase of the number of subcarriers of transmitting effective information, the error detection probability of the receiving end increases, bringing a certain error code loss.③With the increase of the turbulence intensity, the code error performance of the system is gradually deteriorated.

The carrier optimization algorithm is introduced into the 3D-O-OFDM-IM system to further optimize the code error performance of the system. Figure 5 shows the bit error rate curve of the system before and after using the carrier optimization algorithm. According to this figure, the bit error performance of the system after using the subcarrier optimization algorithm is better than the system without the subcarrier optimization algorithm.

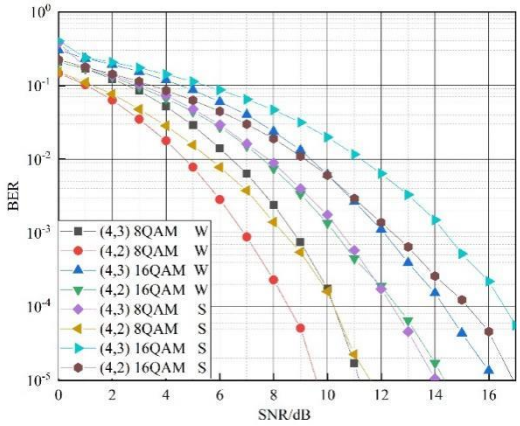

Figure 4 Effect of activator carriers, modulation order, and turbulence on the performance of system error codes

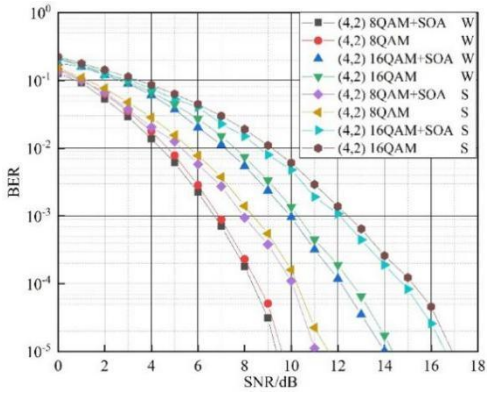

Figure 5 The bit error rate curve of the system before and after using the carrier optimization algorithm

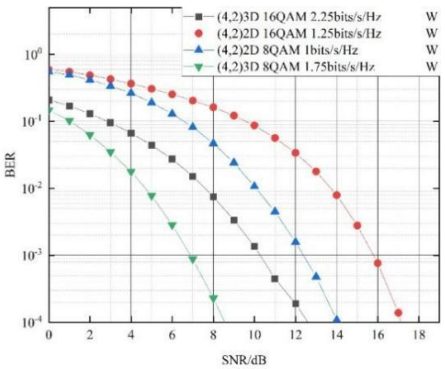

Figure 6 Code error rate under different systems

Figure 6 shows the BER curves for the different systems. According to Figure 6, the bit error rate of the 3D-O-OFDM-IM system is significantly better than that of the 2D-O-OFDM-IM system, because the 3D increases the Euclidean distance between symbols and reduces the probability of symbols being misjudged.

4. Conclusion

In order to realize the communication system with higher reliability, this paper proposes the 3D-O-OFDM-IM scheme by optimizing the traditional constellation symbols. Simulations analyze the code error performance of the system under the exponential Weibull turbulence channel. The results show that the 3D-O-OFDM-IM system has greatly improved the code error performance compared with other systems, and the transmission rate is also improved.

Acknowledgements

Construction Funds for University-Level First-Class Undergraduate (Pilot) Major.

References

[1] ABU-ALHIGA R, HAAS H. Subcarrier-index modulation OFDM; proceedings of the Proceedings of the IEEE 20th International Symposium on Personal, Indoor and Mobile Radio Communications, PIMRC 2009, 13-16 September 2009, Tokyo, Japan, F, 2009 [C].

[2] BAŞAR E A, ERDAL P,ET AL.POOR, H VINCENT Orthogonal frequency division multiplexing with index modulation [J]. IEEE Transactions on signal processing, 2013, 61(22): 5536-5549.

[3] BAŞAR E P E. Optical OFDM with index modulation for visible light communications; proceedings of the 2015 4th International Workshop on Optical Wireless Communications (IWOW), F, 2015 [C]. IEEE.

[4] ZHENG D, ZHANG H, SONG J. OFDM with differential index modulation for visible light communication [J]. IEEE Photonics Journal, 2020, 12(1): 1-8.

[5] YESILKAYA A, BASAR E, MIRAMIRKHANI F, et al. Optical MIMO-OFDM with Generalized LED Index Modulation [J]. IEEE Transactions on Communications,2017, 65(8): 3429-3441.

[6] Ke Xi Zheng Liang, Xu Dongsheng, et al. Research progress of pulse position modulation technology for wireless optical communication [J]. Photoelectric Engineering, 2022,49 (3): 19.

[7] Liu Xu-chao Wen, Li Shaobo, and Sun Shilun. Study on quantum key distribution rate of continuous variable under turbulent channel [J]. China Laser, 2022:1-17.

[8] LE-TRAN M, KIM S. Deep Learning-Assisted Index estimator for generalized LED index modulation OFDM in visible light communication; proceedings of the Photonics, F, 2021 [C]. Multidisciplinary Digital Publishing Institute.

[9] XIAO Y, WANG S, DAN L, et al. OFDM with interleaved subcarrier-index modulation [J]. IEEE Communications Letters, 2014, 18(8): 1447-1450.

[10] MA Q, XIAO Y, DAN L, et al. Subcarrier allocation for OFDM with index modulation [J]. 2016, 20(7): 1469-1472.

[11] Wang Huiqin, Dou Hongxia. Generalized index modulation of asymmetric confined-light in the atmospheric turbulence channel OFDM [J]. Optical Precision Engineering, 2021,29 (9): 2268.

[12] Wang Huiqin, Yang Lirong, Peng Qingbin, Cao Minghua, Chen Dan. The O-OFDM-IM [J] based on a discrete wavelet transform. Journal of Beijing University of Posts and Telecommunications, 2022,45 (3): 57.

[13] BARRIOS R, DIOS F. Exponentiated Weibull model for the irradiance probability density function of a laser beam propagating through atmospheric turbulence [J]. Optics Laser Technology, 2013, 45: 13-20.